

Roving on Ice: Field Testing an Ice Screw End Effector and Sample Collection Tool

Aaron Curtis
Jet Propulsion Laboratory
4800 Oak Grove Dr.
Pasadena, CA 91109
703 303 8060
Aaron.Curtis@jpl.nasa.gov

Matt Martone
Carnegie Mellon University
5000 Forbes Ave.
Pittsburgh, PA 15213
201 625 3362
mmartone@andrew.cmu.edu

Aaron Parness
Jet Propulsion Laboratory
4800 Oak Grove Dr.
Pasadena, CA 91109
818 393 2236
Aaron.Parness@jpl.nasa.gov

Abstract—Icy moons are tantalizing environments in which to search for life beyond Earth and understand the workings of the solar system. However, they pose new challenges for exploration. The low gravity, unknown terrain complexity, and desire to go below the surface (ideally to a water ocean) require new robotic mobility systems for viable roving.

We present the iterative development of an Ice Screw End Effector (ISEE). Using an actuated alpinist ice screw, the tool can support a 250N load in glacial ice as the hand/foot of a climbing rover while simultaneously extracting 1.4cm diameter ice cores. These smaller, more manageable cores can replace monolithic ice cores for collection in inhospitable terrain where robotic access is required.

The collection and analysis of ice cores can explain climate trends, show changes in pollution levels, document extremophile life, and reveal volcanic activity. A sequence of small cores could be collected from various stratigraphic layers by a climbing robot that can ascend sheer ice walls, descend crevasses, or maneuver across the ceilings of ice caves. This low-mass, spatially distributed ice collection strategy presents the opportunity for new paradigms in ice collection, such as 2D grid sampling from ice cliffs, horizontal collection of material along ice strata, and low-impact sampling in biologically sensitive areas.

We present the motivation, electromechanical design, and testing results for the ISEE and discuss the findings of the recent deployment of the tool. The required weight on bit for various densities and temperatures of ice tested in the laboratory is presented and a force-control loop for modulating this value is demonstrated. A mechanism for sample transfer is described along with a simple sample caching architecture. Descriptions of the field sites and samples obtained is also included. We outline a path forward for future tool iteration and prospective robotic integration for the next series of deployments.

1. INTRODUCTION	1
2. BACKGROUND	2
3. DESIGN AND DEVELOPMENT	6
4. TESTING AND RESULTS.....	10
5. DISCUSSION AND CONCLUSIONS.....	13
ACKNOWLEDGEMENTS.....	14
REFERENCES	14
BIOGRAPHY	16

1. INTRODUCTION

The ongoing search for extraterrestrial life centers on first confirming the presence of water, followed by scanning for organic carbon and other building blocks of cellular organisms. On the dusty expanses of Mars, the most frequent site of planetary robotic exploration, the search is limited to geological surveys of areas that have been dry for millions of years. Recently, focus has shifted to cryoic moons such as Europa and Enceladus. These frozen worlds are home to some of the most exotic landforms in the solar system; crevassed ice crusts dotted with potential cryovolcanoes over liquid water oceans. These oceans have the potential to house microbial life similar to that of Earth's primordial oceans, but their alien terrain poses challenges for robotic roving.

Planetary rover missions generally involve surface exploration (mobility) and scientific analysis. Often, these two tasks are accomplished with separate subsystems, usually a drive train with an instrument payload. The Ice Screw End Effector (ISEE) makes use of an alpinist ice screw to combine locomotion and sampling into a single subsystem for gravity-independent traversal of icy worlds. Intended for use on a limbed climbing robot, the ISEE can anchor to glacial ice and support large loads in tension, compression, and bending,

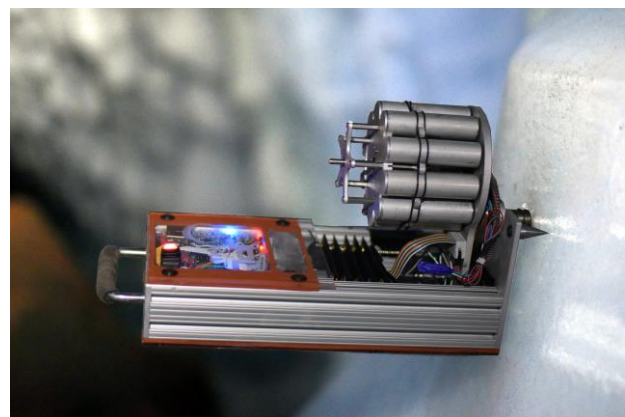


Figure 1: The completed ISEE 2 deployed in an ice cave on Mt. Rainier.

enabling a rover to cling to ice walls at any angle. Additionally, using the hollow-centered ice screw, a core sample is extracted and can be cached or analyzed with each step.

The ISEE has undergone two major iterations over the last year of development, from a proof of concept ISEE 1 to a prototype ISEE 2 (Figure 1) that expanded core caching and information collection abilities. Each prototype was tested extensively in a lab setting as well as on field tests to Mt. Erebus in Antarctica and Mt. Rainier in Washington State. While additional maturation is needed, preliminary testing shows the tool's viability for future icy world missions.

2. BACKGROUND

ISEE's ice climbing, sample collection, and caching capabilities were tailored to the ice types on which it will operate and the scientific questions it will address. ISEE is envisioned to provide mobility on two of the solar system's most promising targets in the search for life: Europa and Enceladus. The discovery of liquid water oceans beneath the water ice crusts of these two outer solar system moons upended the notion that the solar system's "habitable zone" ends at the orbit of Mars [1]. Burgeoning interest in these two objects recently led to the creation of the NASA's Ocean Worlds Exploration Program, the formulation of the Europa Clipper mission, and intense research into mission designs for a Europa lander and Enceladus flyby missions. Both worlds receive significant heating from tidal processes related to orbital resonance with other moons, which may be combined with other thermal sources such as serpentinization, radioactive decay, and residual heat of accretion. Intense tectonic activity and active cryovolcanism have produced deeply dissected, ice-boulder-strewn surfaces, especially in the regions of greatest scientific interest (Figure 2) [2], [3].

Enceladus, a 500-km diameter moon of Saturn, continuously emits a plume of water ice, gases, salts, and simple organic molecules, through geyser-like fissures located in the "tiger stripes" region at its south pole, coincident with a localized hot spot emitting 3 to 7 GW [4]. The jets are sourced, either directly or indirectly, from the subsurface liquid water ocean. Compelling habitability questions would be answered by obtaining samples from the ocean which have been minimally modified by transport processes. The need to access the ocean has given rise to several mission concepts which propose melting through the icy crust, which is tens of kilometers thick [5], [6]. However, we favor the recent approach taken by [7], which proposes travelling down the fissures rather than melting through the crust. That study compared several approaches for Enceladus fissure descent and concluded that an ice screw equipped climbing robot was the most appropriate platform.

Jupiter's moon Europa is strongly suspected to emit similar plumes based on observations by Earth-based telescopes [8].

Europa lacks structures that are directly analogous to the Enceladus "tiger stripes," but the surface is covered in lineae which are thought to result from extensional tectonic processes bringing younger ice mantle material to the surface [3]. An exploration mission to Europa was identified as the second highest priority after a new Mars rover in the National Academy of Sciences' 2013-2022 planetary science decadal survey [9].

Mobility on Enceladus or Europa requires a gravity-agnostic approach. The gravitational constants at the surface of those bodies, 0.0113 g and 0.134 g respectively, are too low to provide the necessary ground pressure to prevent slipping on a wheeled rover like the rocker-bogie systems used on Mars. A mission attempting descent into the Enceladus vent fissures will encounter "upward" dynamic pressure resulting from plume flow that overwhelms the "downward" pull of gravity. Such a mission may be required to climb against the vent flow, rather than rappelling or dropping into the vent, depending on the size of the flow and resultant dynamic pressure.

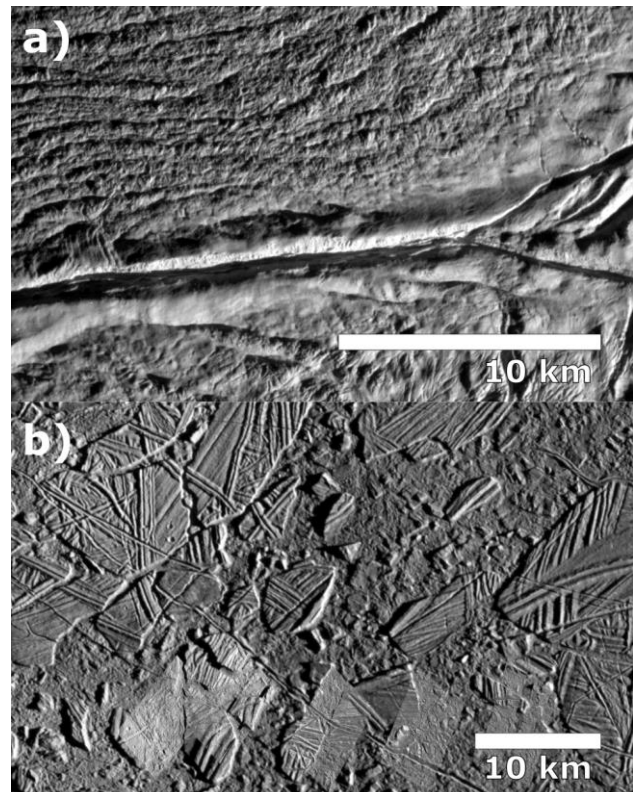


Figure 2: a) Damascus Sulcus tiger stripe on Enceladus b) A mosaic of Comnamra Chaos on Europa, assembled from images taken in 1997 by Galileo's SSI instrument (PIA01403)

A) Ice sample collection

Collection of an ice sample from the surface of a planetary body has never been attempted beyond Earth (except for the permafrost trench sample collected by the Mars Phoenix lander). On Earth, cores retrieved from Greenland and Antarctica are an invaluable source of paleoclimate information dating back as far as 2.7 million years [10]. Typically, such cores are about 10 cm in diameter and can be as long as 3.2 km [11]. Well-established core processing methods exist for investigating particles in the ice such as volcanic material and windblown dust, gases trapped in bubbles in the ice, and the chemistry of the ice itself. These methods often remove material on the outside of the core, taking advantage of favorable preservation conditions afforded by the relatively large diameter core.

When sampling ice from a planetary mission platform, new techniques will be required. Launch volume and mission power limitations make drilling a deep, large diameter core infeasible for the foreseeable future. Thus, sample collection and processing chains for small samples must be developed. Instead of drilling to significant depth, a rover which can obtain small samples from a wide range of sites is preferred. It is possible to emulate a deep core by travelling to sites where ice of different ages is exposed at the surface – a method known as “horizontal coring” and occasionally employed on Earth [12].

Techniques for geochemistry and life detection on small samples are not well-developed or validated. However, total organic carbon (TOC) is commonly used as an indicator of the habitability and/or bioburden of a sample. TOC analysis has been applied to traditional ice cores [13] and snow samples [14], and we decided to adapt existing methods for small cores and conduct such an analysis using ISEE during our Mt. Rainier field campaign (Section 4D).

B) Earth science targets: fumarolic ice caves

Icy landforms on Earth represent analogs to our planetary exploration targets, but are also of scientific interest in their own right. An estimated 20.3% of recently active volcanoes host persistent ice masses [15]. Volcano-ice interaction processes sustain microbial oases on cold, dry, UV-blasted summits which would otherwise be barren. The genetic makeup and microecology of the extremophiles inhabiting these areas informs our knowledge of the deep history of life [16]. As planetary analogs, these sites continue to expand our definition of what constitutes the habitable zone in our solar system. We selected fumarolic ice caves at two such sites for field testing ISEE: the summit craters of Mt. Erebus, Antarctica, and Mt. Rainier, Washington.

The summit caldera of Mt. Erebus, the world's southernmost active volcano, is dotted with hundreds of geothermal features. Depending on details of the specific local snow accumulation regime, three major feature types form: warm ground, fumarolic ice towers, and horizontally developed

fumarolic ice caves (Figure 3). The discovery of life in the warm ground areas sparked astrobiologists' interest in these geothermally heated Antarctic oases [17]. The search for extremophiles in the fumarolic ice caves are of particular interest because as “Dark Oligotrophic Volcanic Environments,” (DOVE) they share several characteristics with deep sea vent and potential planetary habitats, including vents on Enceladus [18], [19]

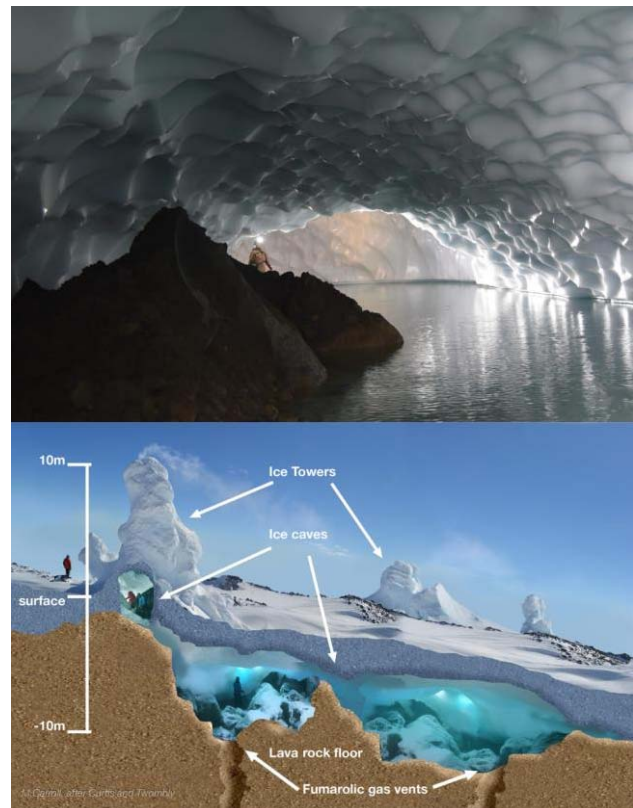


Figure 3: Fumarolic ice caves. Above: Adelie Lake, Mt Rainier, Washington. Below: Diagram based on fumarolic ice caves and towers of Mt. Erebus, Antarctica.

Table 1: Summary of fumarolic ice cave field sites, including two visited in the course of this work

Fumarolic ice cave site	Logistics	Permission required / protection	Caves	Life	Hazardous gases
Mt Erebus, Ross Island, Antarctica (Results from this site presented in section IV)	Short helicopter trip from McMurdo station. Easy access to caves by snowmobiles. Variety of cave entrances: some vertical and some walk-in.	With US Antarctic Program support and standard environmental impact statement process, no special permission required.	Between 100 and 200 significant ice caves. Large diversity in form.	Native bacteria [16]. Contaminant fungi [20]. Possible of microscopic animals [21].	0.5% to 2% CO ₂ (OK)
Mt Rainier, Washington, USA (Results from this site presented in section IV)	Strenuous 2-day climb. Helicopters require special permission. Walk-in entrances.	Permit from park service required to conduct science in park.	One enormous cave with ~8 entrances containing a lake (E. Crater) and a second large cave (W. Crater).	Unknown	1% CO ₂ in East Cave (OK), up to 6% CO ₂ in West Cave (Not OK)
Mt St Helens, Washington, USA	Easy helicopter access, technical vertical cave entry	Managed by US Forest Service rather than Park Service, helicopter permission obtainable.	Several large caves.	Unknown	Elevated CO ₂ but not dangerous
Mt Meager, British Columbia, Canada	Easy helicopter access, technical vertical cave entry	Unrestricted	One large cave entrance. No one has yet entered.	Unknown	200 ppm H ₂ S (deadly)
Mt Rittman, Terra Nova Bay, Antarctica	Access from Jang Bogo or Mario Zuchelli station; requires collaboration with South Korea or Italy. Further than Melbourne; Requires fixed wing	Antarctic Specially Protected Area No. 175	Steaming fumaroles. Unclear what caves and towers may exist.	Bare ground areas host diverse life	Elevated CO ₂ but not dangerous
Mt Melbourne, Terra Nova Bay, Antarctica	Helicopter access from Jang Bogo or Mario Zuchelli station; requires collaboration with South Korea or Italy	Antarctic Specially Protected Area No. 118	Several ice towers	Bare ground areas near caves host diverse life. Leafy moss. New species <i>Bacillus thermoantarcticus</i> discovered here	Elevated CO ₂ but not dangerous
Mt Berlin, Marie Byrd Land, Antarctica	Extremely remote. Need USAP deep field camp.	Unrestricted	At least one large ice tower	Unknown	Unknown

C) *Properties of ice relevant to climbing*

In the planetary landscapes ISEE may someday roam, ice exists in a staggering range of chemical compositions and physical structures and at a vast range of temperatures and pressures. Someday, landed missions must explore such exotic ices as the CO-CH₄-NH₄-laced nitrogen ice planitia of Pluto and seasonal CO₂ ice on Mars [20], [21]. In the near term, the solar system’s most abundant ice, H₂O, is of more interest. Water ice dominates the surface of the two most promising candidates in our search for life – Saturn’s moon Enceladus, and Jupiter’s moon Europa. The Martian residual polar ice caps are also primarily water ice, and of course Earth hosts icy landscapes of great scientific interest. Water ice can exist in at least seventeen distinct crystal phases, as well as several amorphous structures, but is mostly present as ice Ih (hexagonal ice) on the worlds of interest to this study.

Thus, while designing and testing ISEE, we considered requirements for anchoring to ice Ih in the temperature and pressure regimes that might be found on Earth, Mars, Enceladus, and Europa. Mechanical properties of ice Ih relevant to climbing, such as its tensile strength, fracture toughness, and hardness, depend on temperature, density, and grain size [22]. ISEE performance was validated in a small subset of this enormous parameter space (Section 4): we tested on freshwater with minimal impurities, between 187K and 273K, at densities between roughly 0.1 and 0.8 g cm³.

Table 2: Target landforms of interest for ice climbing

Formation mechanism	Landforms to climb
Snow-like falling precipitation & subsequent diagenesis	Earth: glaciers
	Enceladus: most of surface [23]
Freezing of liquid water ocean (and subsequent solid phase transport)	Europa: most of surface
	Earth: sea ice
Deposition of frost (direct vapor-to-solid phase change)	Earth: hoarfrost
	Mars: North polar layered deposits

Natural ices of interest for robotic mobility on Earth and Enceladus are initially deposited from the atmosphere, either as snow or by deposition (direct vapor-to-solid phase change) as in hoarfrost. Snow on Enceladus is thought to consist of sub-micron to 100-micron diameter grains [24]. Snow diagenesis processes on Enceladus, such as sintering, compaction, and regelation, are probably as complex and various as those of Earth, but are not yet understood in detail. However, Ono et al. posits that walls in active vents, exposed

to impacts from plume ice grains and gas flow, are subjected to processes that strengthen and densify the ice mass [7]. Cassini Imaging Science Subsystem measurements also suggest larger grain sizes within the tiger stripes compared to the interstripe plains, and does not preclude that the surface within the tiger stripes may be “boulders composed of coarse-grained ice crystals” or “relatively bare outcrops of solid ice” [25].

When ice climbing using a screw, there are three actions of interest: screw placement, body shift, and screw removal. The mechanical design must consider each phase and the required mechanical properties of ice (Table 3).

Table 3: Mechanical properties of ice relevant during phases of climbing gait sequence

	Fracture toughness	Shear strength	Hardness	Tensile strength	Friction
Screw placement	■	■	■	■	■
Body shift	■	■	■	■	■
Screw removal	■	■	■	■	■

For successful screw placement, screw teeth must dislodge sufficient ice to create a cylindrical bore, and then screw threads must cut into the bore walls. Dislodging ice grains is primarily a brittle process, but may involve initial plastic deformation. Fracture toughness and shear strength of ice increase significantly with densification from snow to ice. For ice formed from liquid water at typical Earth temperatures, those values are: 50 to 150 kPa m^{1/2} and 0.7 to 3.1 MPa, respectively [22]. Ice tensile strength, toughness, and hardness are relatively insensitive to temperature, with a slight increase as temperature decreases [22], [26]. Shear strength and tensile strength are nearly equal for dense snow [27].

In the loading phase, the anchor formed by a placed screw must be able to react the downward force resulting from robot’s upward body shift to the next foot placement point, and then the outward force resulting from weight on bit applied during the next screw placement. Failure during this phase is unlikely because ISEE 1 and 2 employ ice screws which are rated to hold loads of 10 kN downward force (tested to an average of 19 kN by [28] in dense, lab-frozen water ice).

Successful ice screw removal requires sufficient torque to overcome frictional forces between the screw threads and

borehole walls. Predicting friction coefficients for ice is complex and requires consideration of a water or water-like layer which forms at the contact boundary layer [29]. The torque values reported below for ice screw removal are related to the coefficient of friction, but not easily converted due to uncertainties in parameters including actual contact area, wettability, and thickness of the lubricating layer.

D) Robotic background

The Ice Screw End Effector is envisioned as the hand/foot of a limbed climbing robot. Microspine grippers [30] and small drills [31] have been developed for rocky planetary surfaces, gecko-like adhesive grippers have been demonstrated for smooth surfaces in microgravity [32], and auger-like drills have been proposed for regolith surfaces on comets and asteroids [33]. However, limited work has been performed for anchoring to icy surfaces. Only Nayar et al. demonstrated a three-fingered gripper that anchored by sublimating ice away with heater [34]. This work shows an alternative approach that also enables sampling with each anchored step.

A limbed robotic system is preferred because the low gravity, terrain complexity, and desire to access vertical vent surfaces preclude the use of wheeled systems. Previously developed high-degree of freedom limbed climbing platforms include the two-limbed dynamic robots [35], [36] four-limbed LEMUR series of robots [37]–[39] and Spinybot platforms [40], the six-limbed RiSE robot [41] and ATHLETE robot [42], and the eight-legged ABIGAILE robot [43] among others.

Robots consisting of a single limb, such as the snake-like robots developed by Choset et al. are also useful also useful design topologies under consideration [44]. These high-dimensional robots are capable of placing a climbing end-effector precisely in any orientation while avoiding obstacles. This makes them optimal for climbing in constrained spaces or uneven terrain such as the inside of a crevasse or a fumarolic ice tower. A snake robot can also react all loads

generated by the ISEE during anchoring and adapt to time-varying gas pressure in any direction [45].

A walking limb [46]–[48], inspired somewhat by an inchworm, is a platform of particular interest. Compared to a multi-limbed robot, a walking limb maximizes the speed of traverse, an important parameter in the radiation limited mission timeline, by requiring only a single step per stride (vs. 4 or more). It can also fit through much narrower gaps as it descends vents or crevasses, yet can still place instruments and sample the terrain with mm-scale accuracy and precision pointing. Using a limb derived from the RoboSimian [49] platform, an example gait sequence for such a system is shown in Figure 4.

3. DESIGN AND DEVELOPMENT

To successfully act as a reliable anchor and scientifically viable sample caching system, the Ice Screw End Effector must be capable of many functionalities (Table 4). While the most basic of these involves anchoring to ice and extracting cores, the future of the ISEE on a potential Europa or Enceladus rover depends on its ability to store interesting samples, preserve sample integrity, and manage unintended environmental interactions without human intervention. Rather than prototyping an ISEE with all functionalities, an iterative approach was used to increase abilities with each version. This allowed us to ensure that the most important functions will be perfected while more peripheral functionalities can be integrated into the system over time.

A) Ice Screw End Effector Version 1

The first operational prototype for ISEE (Figure 5) was designed to demonstrate automatic placement of an ice screw and to support loads expected for climbing if the ISEE was mounted on the LEMUR 3 climbing robot [39]. In the ISEE 1 design, a motorized ice screw assembly is attached to a ball bearing carriage that rides on a linear rail. The rail allows the carriage to be pulled forward relative to the front plate and lower housing by the self-tapping ice screw during insertion.

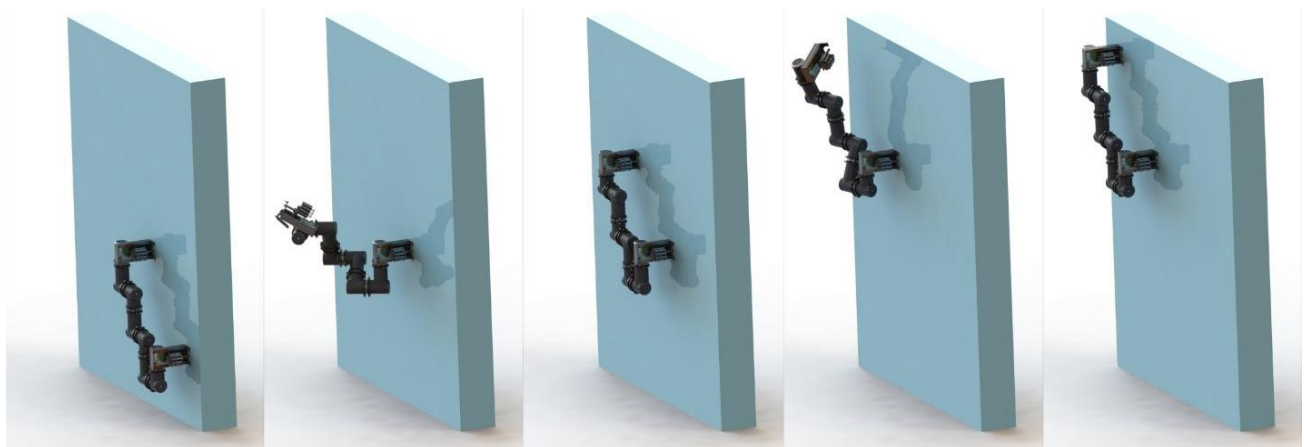


Figure 4: An "inchworm" robot, one possible climbing system using ISEE.

Table 4: Functionality chart of the existing ISEE versions.

Functionality	ISEE 1	ISEE 2
Repeated Sampling	✓	✓
Wall/Ceiling Ice Anchor	✓	✓
Clear Clogged Screw	✗	✓
Cache Multiple Samples	✗	✓
Measure Weight-on-Bit	✗	✓

The ice screw carriage assembly consists of a shaft supported by a tapered roller bearing at each end. Because ice cuttings must flow through the shaft during operation, the shaft is hollow, with an internal diameter slightly greater than that of the ice screw. At the aft end of the shaft, a retaining ring supports a wave spring which provides preload for the tapered roller bearings. At the forward end, the shaft diameter increases to form the ice screw mount and to retain the main drive spur gear.

Prior to ISEE 1 development, mechanical connections to COTS ice screws did exist, but none were designed as part of the load path for climbing. DLR’s IceMole melt probe employs an ice screw to pull the heating pads into contact with the ice, but details of that attachment are not available and it is not clear if it would be appropriate for the large wall-parallel load vectors we expect [50]. A patent for a power drill adapter enabling human climbers to quickly insert ice screws was also found [51]. It was designed to allow quick insertion and removal, and transmit screw placement torque and weight on bit, but not to support loads through the ice screw attachment assembly.

The ISEE 1 ice screw mount uses clamps to interface to flat surfaces on the back of the ice screw. Ice screws are manufactured with these flats to transmit torque from the ice screw handle. We cut away the handle before mounting the ice screw. The screw must be manually centered when mounting. We improved the ice screw mount in ISEE 2 to reduce the possibility of misalignment during mounting (Section 3B).

ISEE 1 has three springs which control contact between and position of the ice screw carriage assembly relative to the linear rail and housing. The front wave spring is compressed when the ice screw is completely inserted, dampening transient forces from climbing acceleration and providing a small amount of compliance. The aft wave spring acts as a simple force gauge for our weight on bit experiments. The ISEE 1 housing, adjacent to the spring, is marked in intervals of 5mm, each representing 60N of weight on bit (the spring constant is 12N mm⁻¹). An extension spring returns the ice screw carriage assembly to the home position for the phase

of the gait in which the ice screw is not interacting with the wall.

The ISEE 1 drive system consists of a 24V brushed DC motor, a planetary gearbox, and a pinon / spur gear pass. The system produces 14.6 Nm at the ice screw, which rotates at 15RPM consuming about 20W during insertion. For our field tests, we built a custom switchbox allowing bidirectional manual control of the ice screw drive motor, with a 3 position switch and flyback protection circuit.

This iteration of ISEE provided valuable insights that would later be redefined into quantitative requirements for the ISEE 2. Testing on various types of ice yielded weight-on-bit (WOB) and screw torque measurements, and field observations such as screw clogging in sub-zero temperatures revealed potential issues that would require new functionalities in future iterations.

B) Ice Screw End Effector Version 2

The ISEE 2 (Figure 6) is a more electromechanically complex tool, with five distinct subsystems, onboard electronics, and three microprocessors. Here we detail the design and functionalities achieved by each major subsystem.

Actuated Lead Screw—ISEE 2 uses a second driven degree of freedom along the axis of the ice screw. A non-backdrivable, actuated lead screw replaced the free-sliding carriage from the ISEE 1 design, allowing the ISEE to extend the screw into the wall at a calculated rate. This effectively



Figure 5: ISEE 1, showing a) 13cm alpinist ice screw b) Ice screw retaining clamps c) Linear rail d) Pinion / spur gear pass e) Planetary gearbox f) 24V DC motor g) Hollow shaft h) Tapered roller bearings i) Extension spring for carriage homing j) Wave spring, compressed to desired weight on bit during ice screw thread initiation k) Force gauge graticule l) Handle for manual operation m) Switch box for manual operation

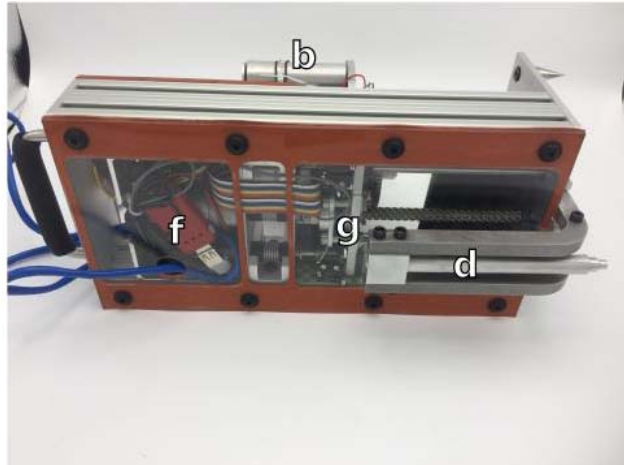
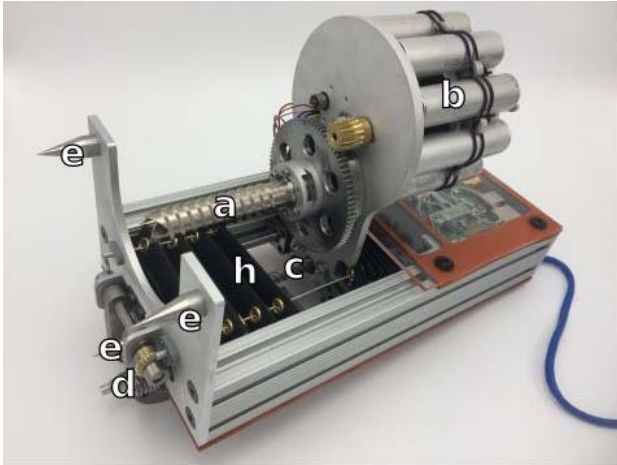


Figure 6: Oblique and rear views of ISEE 2 prior to the Mt. Rainier deployment, showing a) COTS alpinist ice screw b) Sample caching carousel c) Lead screw drive d) Sample clearing rod e) Ice spikes to react off-axis loads f) Sealed electronics compartment g) Weight on bit sensor h) Accordion ice ingress protector (partially removed)

splits the ISEE mechanism into two major portions, a waterproof housing for electronics and motors and a moving carriage that contains the ice screw and core-caching system.

The lead screw system applies torque and weight on bit to the screw through a center shaft and reacts cross moments and side loads through parallel rails. These two parallel rails with linear bearings are included on either side of the lead screw to fully constrain the motion to one dimensional linear travel along the rails when the lead screw is turned. To limit overconstraint, one rail is seated in fixed bearings on both ends while the second uses a flexible shaft coupler, preventing binding.

The lead screw is a 3/8" outer diameter 5-start precision screw, which is optimized for fast yet precise linear actuation. The subsystem is actuated by a Pololu 6V brushed DC motor capable of a max torque of 1.57 Nm, which translates to an approximate maximum output force of 200 N. This keeps the screw preloaded into the wall during initial anchoring, then keeps the screw moving along its self-tapping trajectory until the anchor is fully set. An encoder reads the position of the motor shaft, which can be used to find the linear position of the carriage. Both ends of travel are also sensed by limit switches on the carriage.

Force-Sensing Floating Nut—Attached to the lead screw subsystem is the carriage plate, which rides along the rails when driven by the screw. This plate is constrained by the linear bearings on the rails and is driven by a nut that couples with the lead screw. The nut is decoupled from the plate along the axis of the lead screw by a linear spring and decoupled in the perpendicular plane by a bolt pattern set in oversized mount holes, allowing the nut to float. This design (Figure 7) ensures that no bending moment can be applied to the lead screw motor assembly, and all torques generated by anchoring or climbing are reacted by the rails.

To measure WOB, a Futek force sensor was placed in series with the spring and floating nut system. In addition to data collection, this sensor is used as input to a force-based control loop that ensures that the ice screw threads are self-tapping and the motor is following along as it is driven into ice. The WOB needed to drill into ice walls is also useful as a science measurement.

Ice Screw Drive—The ice screw drive system design topology remains largely similar to the ISEE 1 system. A Pololu 12V brushed DC motor drives the ice screw. The motor is geared down with a 3:17 ratio to increase the torque with which the ice screw taps into the ice wall.

The ice screw mounting hardware has been significantly redesigned such that the screw is automatically centered on the gear's axis when clamped. The output gear and screw mount assembly is fastened to the carriage via a cross roller

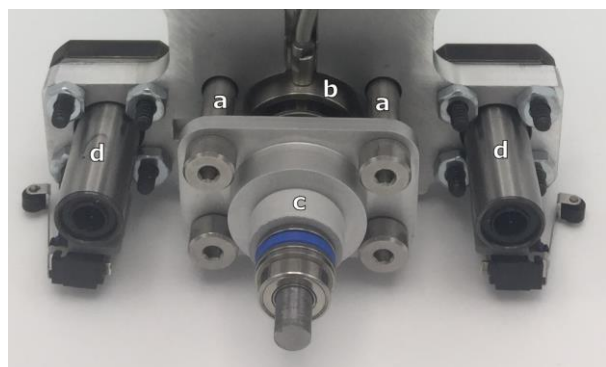


Figure 7: Force-sensing floating nut assembly showing a) Shoulder bolts with oversized mount holes b) FUTEK force sensor c) Lead screw precision nut d) Linear rail bearings.

bearing, which can support all loads the ice screw is designed for.

Core Caching Carousel— ISEE 2 includes a core caching system able to store ten cores simultaneously in an actuated carousel. In this iteration, the caching tubes are not sealed; avoiding cross-contamination requires that significant portions of sample are melted away before analysis. Cores are simply constrained by a plate covering the mouth of the tube, and can be retrieved by manually removing the tube.

The carousel is equipped with a rotary absolute encoder that allows the ISEE to move to set positions, ensuring that the correct capsule is selected at any given time. To reject an uninteresting sample, one capsule can be omitted during deployment, creating a ‘dump slot’ that allows the extraneous core to fall out the back of the system. For a roving system that will take thousands of steps (and thus takes thousands of core samples), this feature will be essential.

Ice Screw Stowing Unclogger— An unclogging mechanism was implemented to force samples into the caching system and remove trapped cores from the inside of the ice screw that prevent future emplacement. This subsystem (Figure 8) is stored under the housing during anchoring, but rotates up into place in the path of the ice screw. Once locked in place, the ISEE pushes the screw forward, forcing the unclogging rod through the screw and ejecting the core into a sample capsule.

The clearing mechanism is deployed by a Pololu 6V brushed DC motor that can provide 0.25 Nm. The loads on the motor are kept low by a non-backdrivable worm gear in the load path. To accommodate spatial and weight constraints, the drive shaft of the motor doubles as one of the rails of the linear deployment system. Final deployment and stowing positions are set by hard stops and a current-control loop on the motor, ensuring that the rod is coaxial with the ice screw to prevent interferences.

Housing and Interface—Though the ISEE will eventually be used on a robot limb for climbing, the ISEE 2 is designed for stand-alone lab and field testing. The housing includes a handle and external buttons for manual control, as well as a



Figure 8: Ice screw clearing mechanism prior to attachment to the ISEE 2.

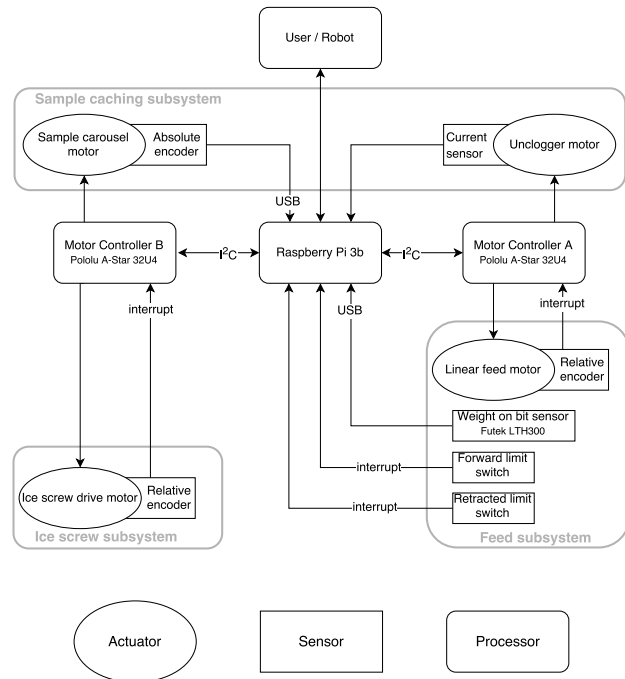


Figure 9: ISEE 2 system architecture

GUI for wireless operation from a nearby computer. The housing is comprised of 80/20 aluminum extrusions with 3/8” thick aluminum end caps, made water resistant with silicone caulking and removable acrylic covers with matching rubber gaskets.

Three sharpened steel spikes at the bottom end of the housing are used to prevent sliding during anchoring when locating the ISEE on a wall. As the screw nears its end of travel, these spikes are driven into the wall, reacting torques around the screw and transferring much of the load from the ice screw actuation system to the walls of the housing.

Control architecture—In the transition from ISEE 1 to ISEE 2, the addition of three actuators and nine sensors came with a concomitant increase in control system complexity (Figure 9). In place of ISEE 1’s three position switchbox, the control system of ISEE 2 consists of three processor boards. All high level code, communications with the operator or parent robot, and data logging occurs on the relatively powerful Raspberry PI 3 Model B (1.2GHz quad core ARM processor). Two Pololu A-Star 32U4 motor controller boards drive two motors each. Each motor controller has considerable processing capability provided by the Atmel ATmega32U4 (16 MHz 8-bit AVR). Communications between the three boards is achieved on a single I²C bus, with the Raspberry PI configured as master and the motor controller boards configured as slaves.

A centralized rather than distributed architecture is used with all control loops and logic run on the Raspberry PI, in Python

3.4 on Debian Jessie-based operating system. Sensors are connected directly to the Raspberry PI except for the relative encoders on the ice screw drive and linear feed motor. These sensors output a quadrature signal, best received using two dedicated processor interrupt pins per encoder. Although it is possible to handle this on the Raspberry Pi's interrupt pins, the encoders will trigger hundreds of interrupts per second during normal operation, leading to significant processor load. Thus, we connected the encoders to the motor controller interrupt pins, count the encoder pulses using code running on their onboard processors, and periodically send sums to the Raspberry PI.

Control code on the motor controllers is C++, using a modified version of the Raspberry Pi slave library for Arduino. Modifications include handling of the motor encoder quadrature and changes to support multiple I²C slaves. The library handles continuously passing packed messages back and forth between the Raspberry Pi and the motor controller board with status and commands.

High level code running on ISEE 2 is implemented in the event-driven application framework Urwid. This allows handling of new data from all sensors upon receipt, logging of all sensor data and application state to an SD card, and a text-based graphical user interface for use during test campaigns. In addition to all sensor values and motor states, the GUI also displays state of health information including system resource utilization and battery voltage. The application is accessed using SSH via ethernet or wireless connection to the Raspberry PI.

It is important to be able to maintain a desired weight on bit force, both for testing and operational purposes. We achieve this using a PID control loop running in Python based on the free ivPID library, with error input sourced from the Futek load cell and output driving the lead screw motor. The ability to reliably maintain a desired weight on bit solves an otherwise problematic mechanical issue. The ice screw is self-tapping, and thus acts as a feed, which must be synchronized with the motorized lead-screw to prevent the generation of significant internal forces. Maintaining a desired WOB is a software solution for ensuring the lead screw feed follows ice screw motion.

C) Future Versions

Several improvements and new capabilities are planned for the next generation of ISEE, for example, sealing sample tubes to prevent cross contamination. Miniaturization and adaptation for mounting to a limbed robot will also be prioritized.

4. TESTING AND RESULTS

A) Requirements Testing

During the prototyping and design of the Ice Screw End Effector version 2, many system requirements were quantified in order to justify material choices, motor torques,

and mechanism designs. Here we detail some of the requirements validation testing for ISEE 2.

Unclogging Force—Many mechanism designs were considered for the unclogging subsystem. The driving factor was the force required to unclog a frozen core, determined by testing on artificially clogged screws. Testing consisted of applying force to a rod inside a clogged screw until the core was cleared. In this way the peak force could be found for each use case (Table 5).

Table 5: Mean unclogging force required to clear screws under different conditions.

Core Condition	Ejection Force (N)
Screw and Ice @ -15°C	2.2
Screw in Ice Overnight	89.0
Core in Screw Overnight	198.9

Core Stratigraphy Integrity—Though the cores extracted through an ice screw are generally solid, it is important to note that their composition is mostly tightly packed firn. The teeth of the ice screw scrape layers of ice during deployment, becoming tightly packed reconstituted ice inside the channel of the screw. For some science objectives, core stratigraphically must be maintained. A series of lab tests on layered ice successfully showed that some layer mixing does occur during core extraction, however the samples stratigraphy integrity is largely preserved on a macro scale (Figure 10).

Carousel rotation—Sample collection and retention depends on precise and reliable rotation of the sample carousel assembly. Rotation is actuated by a brushed DC motor controlled using a PID loop which takes positional input from a magnetic ring absolute encoder. To verify operation, we simulated a sample collection scenario in which the carousel rotates to the dump position between each sample collection,



Figure 10: A core sampled from multilayer colored ice during lab testing that shows that the bottom layer (red) remains largely unmixed with the top layer (blue).

so that the sequence is: 0 (dump position), clockwise to 1, counterclockwise to 0, clockwise to 2, counterclockwise to 0, and so forth to tube 9. Alternating the direction of rotation avoids sample leakage that could occur if a filled sample tube is rotated past the ice screw position. We ran the full sample collection scenario 10 times and obtained the results shown in Figure 11 and Table 6. At a 95% confidence level, we verified that the movement from dump position to the sample tube reached the correct tube alignment with a maximum rotary error of $\pm 3\%$ of the rotation distance between 2 tubes. The low standard deviations indicate that the motion is highly repeatable (excellent precision, despite moderate trueness), indicating that further PID loop tuning could greatly reduce the 3% error. At any rate, 3% is sufficient to avoid any loss of sample.

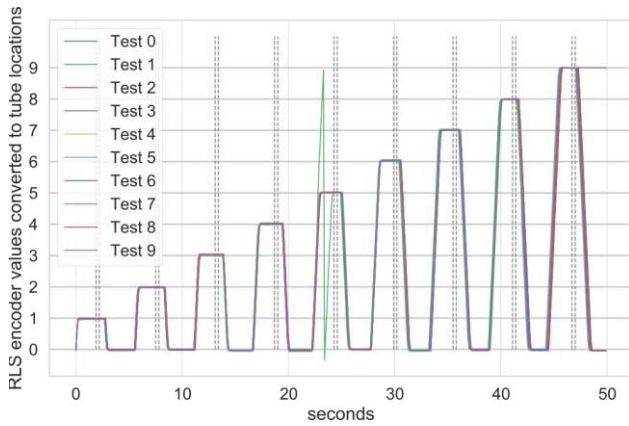


Figure 11: Encoder output during carousel rotation performance test. Dotted lines indicate “end position” data used to calculate values in Table 5

Table 6: Results of carousel rotation performance test

Move	Mean end position	Standard deviation	Confidence (\pm) @ 95%
0 to 1	0.97	0.0123	0.0076
0 to 2	1.98	0.0063	0.0039
0 to 3	3.01	0.0165	0.0102
0 to 4	4.01	0.0158	0.0098
0 to 5	5.01	0.0120	0.0074
0 to 6	6.03	0.0135	0.0084
0 to 7	7.01	0.0149	0.0092
0 to 8	7.99	0.0103	0.0064
0 to 9	9.00	0.0067	0.0042

B) Force-torque testing

To test WOB values across a broader range of variables and to obtain measurements of torque required to sustain screw rotation, we assembled a test stand, shown in Figure 12, based on an ATI 6-axis force-torque sensor (Gamma). Both ISEE 1 and 2 can be mounted on this test stand, and drill into a block of ice affixed to the force-torque sensor. Because ISEE 1 lacks a feed system to apply WOB, we fabricated an adapter to allow weights to be placed on the ISEE sample carriage, driving it downwards into the ice sample using gravity. Additionally, we added a linear potentiometer to measure the carriage position for ISEE 1 tests. We digitized the force-torque sensor and linear potentiometer output using a National Instruments USB-6211 DAQ and displayed live and recorded data using python code we developed.

Ice blocks were frozen from deionized water poured into a 4-quart Tupperware container and placed in a chest freezer for 48 hours. All ice was initially frozen in a -20 C freezer. For cryo-ice tests, we then moved the samples into a -86 C freezer for a further 48 hours. We produced reduced density ice by starting with carbonated water.

Torques imparted on the ice by the screw during experiments generally peaked between 1 and 4 Nm (Figure 13). By observing the change in torque, it is possible to gain some insight into the process of thread stripping and the resulting failure of screw insertion. In Figure 13b, we see transmitted torque decrease after threads are destroyed at 1.25 Nm.

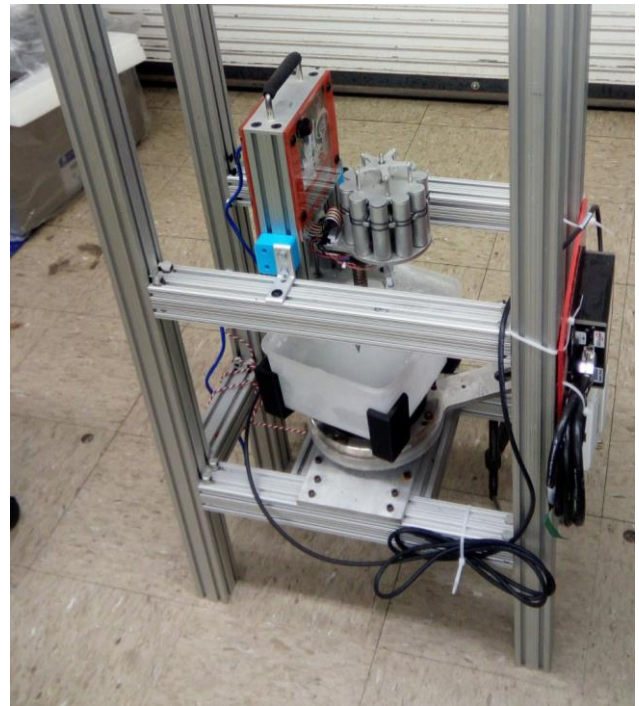


Figure 12: Force-torque test stand with ISEE 2 mounted

WOB was the primary variable, but we have also conducted experiments to investigate several other parameters. Using ISEE 1, we varied rotation rate independently of WOB (Figure 14). We have also begun to investigate the effects of ice parameters including ice temperature, ice density, and granularity. Density and granularity are challenging to vary in the lab, so our experience with these variables is primarily achieved by testing on natural ices in the field.

C) Operational validation: Mt. Erebus, Antarctica

To verify the capabilities presented in Table 4, we conducted field campaigns in natural ice environments of interest for earth science and as planetary analogs. In December 2016, we tested ISEE 1 at various sites in the summit caldera of Mt Erebus, Antarctica: three fumarolic ice caves and a fumarolic ice tower. Objectives of the test were to determine the WOB required to initiate screw insertion, verify the load bearing capability of the anchor, and test performance on the range of natural ice types available in the fumarolic ice caves and ice towers. The ISEE prototype was held against the wall by hand and supplied with a given WOB, controlled by compressing a wave spring that had graduated markings. For each experiment, screw insertion was re-attempted at increasing WOB (30N, 60N, 120N and 180N) until the successfully

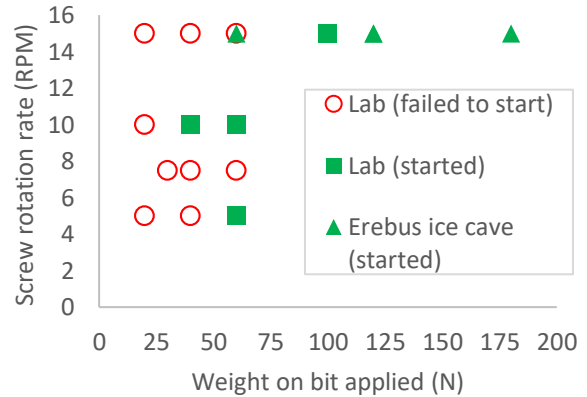


Figure 14: Success or failure of ice screw initiation at a range of WOB values and screw rotation rates

initiated. Each re-attempt was conducted in the same type of ice 10 cm away from the previous insertion. Following anchoring, load bearing capacity to 350 N was verified using a load cell pulled both in the wall-normal direction and a wall-perpendicular direction. We conducted tests at three dense ice sites, and a hoarfrost area in an ice cave wall in Cathedral Cave (Figure 15).

All three tests conducted in dense ice resulted in successful screw insertion with greater than 350 N load bearing capacity (Table 7). WOB requirement for insertion varied from 60 to 180 N. A fourth test in hoarfrost crystals growing on a cave wall failed due to poor coupling with the wall. The screw could be easily inserted into and removed from the wall with no rotation. This highlights a potential concern for descent into vents on icy moons – accumulation of hoarfrost may

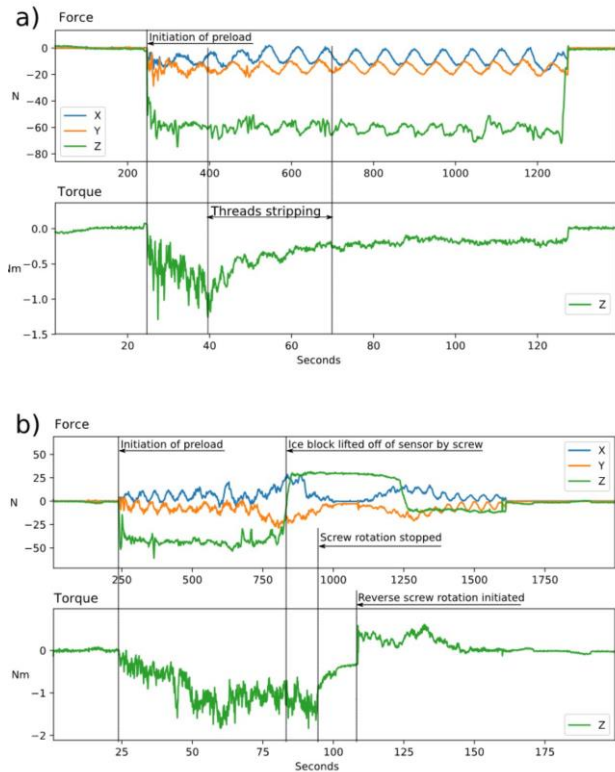


Figure 13: Two examples force-torque datasets during ice screw insertion. a) Failure due to insufficient preload b) Successful anchoring.

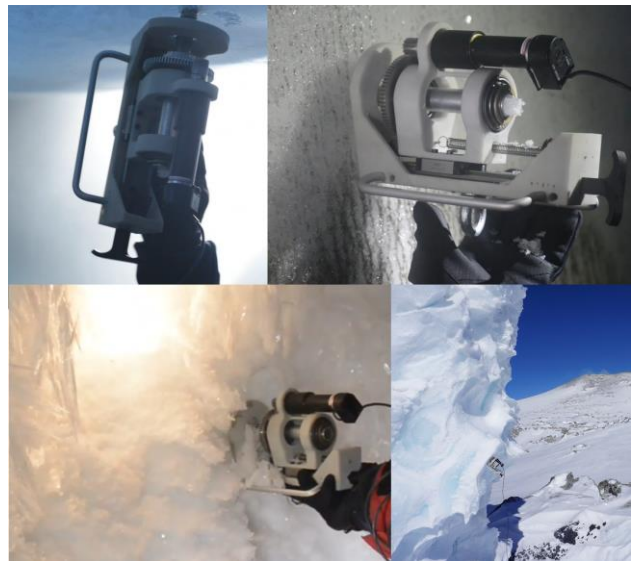


Figure 15: ISEE 1 operational validation in Mt Erebus fumarolic ice caves

prevent effective anchoring. An additional concern was noted: ice became frozen into the ice screw following the test at the Miss Piggy tower, preventing subsequent insertion attempts. This observation raised the priority of

implementing the unclogger mechanism on subsequent iterations of ISEE.

D) Operational validation: Mt. Rainier, WA, USA

In July, 2017 ISEE 2 was tested in the fumarolic ice cave inside the East Crater of Mt Rainier, Washington (Figure 16). The Rainier field campaign sought to verify operation of the new capabilities added to ISEE 2 (Table 4) and to collect TOC samples as described in Section 2A. ISEE 1 was also tested for WOB insertion levels in this new environment. Both ISEE 1 and 2 demonstrated successful anchoring in a range of ice material, including consolidated snowpack (Figure 16d) and glacial ice from near Adelie Lake (Figure 16c). WOB required to initiate the ice screw insertion was lower than expected, less than 60 N. ISEE 2 also successfully demonstrated its sample caching and screw clearing system, which can collect up to 10 samples.

TOC sample collection was also successful. 15 ice samples were collected from a range of stratigraphic levels in the cave walls. We transferred the samples to 20mL screwcap vials for transport. The samples were successfully transported in a frozen state all the way to JPL using a vacuum flask filled with CO₂ ice. They will be analyzed for TOC following the persulfate-ultraviolet method (SMEWW 5310 C) [52].

5. DISCUSSION AND CONCLUSIONS

In the ISEE, we have demonstrated a technology that would enable mobility on icy worlds. Such a rover could achieve scientific objectives literally out of the reach of a static lander. Our small core sample caching methods are a viable method for collecting a “horizontal ice core” using depth as a



Figure 16: ISEE operational validation on Mt Rainier, showing a) Full functionality test of ISEE 2 b) Load bearing test of both 1 and 2 c) ISEE 1 test at Adelie Lake, highest body of water in North America d) Anchoring test of 2 in surface snow

Table 7: Results of ISEE 1 WOB testing in Erebus fumarolic ice caves

Location	Ice type	Ambient T (C)	Test orientation	Min. WOB for screw placement	Load
Hut Cave, Erebus	Dense but white; mm-scale grains	~0	Horizontal	< 60N	> 350N
Hut Cave, Erebus	Near pure; no grain boundaries visible	~0	Horizontal	180N	> 350N
Helo Cave, Erebus	Near pure; no grain boundaries visible	~0	Vertical	120N	> 350N
Cathedral Cave, Erebus	Just beneath 40cm C-axis xtals	-3	Horizontal	N/A	N/A
Miss Piggy Tower, Erebus	Near pure; no grain boundaries visible	-23	Horizontal	120N	> 350N
East Crater Cave, Rainier	Dense but white; mm-scale grains	~0	Horizontal	< 60N	> 350N
Surface of East Crater, Rainier	10cm-scale sastrugi	Not known	Horizontal	< 60N	> 350N

proxy for time. Moreover, observing from a mobile platform allows detection of spatially sparse phenomena such as meteorites, erratics, and tephra layers. When phenomena are spatially diverse (as we know boulder frequency, ice type, and heat flux to be on Enceladus) roving reduces the chance of making spurious measurements of an anomalous area. Signs of life and evidence for habitability on an icy world are likely to be both spatially sparse and diverse, we see mobility as imperative in the search for life.

Lab and field testing showed that of the design constraints placed upon an ice climbing robot, establishing sufficient WOB during the ice screw placement phase of the gait is likely to be of most concern, as opposed to generating sufficient torque for the insertion or removal phases of the gait or supporting the body shift phase. We varied several ice parameters affecting the required WOB, but the most significant factor appears to be granularity of the ice. Polycrystalline ice with small crystal domains, such as that encountered in the wall of Hut Cave, Mt Erebus, and throughout the caves of Mt Rainier, never required more than 60N WOB for successful ice screw placement. Conversely, clear, nearly monocrystalline ice such as that produced in the lab and formed by regelation of drip water on Erebus cave ceilings required WOB as high as 180 N for screw placement.

We were able to apply ISEE's core collection method to collect samples suitable for measurement of total organic carbon concentration values and gradients in the ice on the summit of Mt Rainier. Analysis of these samples is ongoing and will be presented in future work. In the near future, we expect to apply an ISEE-equipped robot to sample inaccessible tephra layers in ice cliffs and crevasses. Further refinements of ISEE core caching capability will broaden the range of scientific questions to which ISEE can be applied. Sterile sampling methods will allow sampling for genetic and microbiological work. We also intend to implement hermetic sealing of sample containers to enable preservation of gasses trapped in the ice cores, which may enable determination of $^3\text{H} / ^3\text{He}$ ratios for age determination and even reconstruction of past atmospheres. Should these investigations prove successful, similar methods could prove appropriate on other icy worlds.

ACKNOWLEDGEMENTS

The research was carried out at the Jet Propulsion Laboratory, California Institute of Technology, under a contract with the National Aeronautics and Space Administration. Copyright 2017 California Institute of Technology. Government sponsorship acknowledged.

Rainier fieldwork was supported by Mt Rainier National Park and facilitated by Eddy Cartaya and Penny Boston of Glacier Cave Explorers. Erebus fieldwork was facilitated by Philip Kyle of the Mount Erebus Volcano Observatory, which is supported by grant ANT-1142083 from the National Science Foundation.

REFERENCES

- [1] J. C. Priscu and K. P. Hand, "Microbial habitability of icy worlds," *Microbe*, vol. 7, pp. 167–172, 2012.
- [2] H. R. Martens, A. P. Ingersoll, S. P. Ewald, P. Helfenstein, and B. Giese, "Spatial distribution of ice blocks on Enceladus and implications for their origin and emplacement," *Icarus*, vol. 245, pp. 162–176, 2015.
- [3] A. C. Barr and N. P. Hammond, "A common origin for ridge-and-trough terrain on icy satellites by sluggish lid convection," *Phys. Earth Planet. Inter.*, vol. 249, no. Supplement C, pp. 18–27, Dec. 2015.
- [4] J. R. Spencer *et al.*, "Cassini Encounters Enceladus: Background and the Discovery of a South Polar Hot Spot," *Science*, vol. 311, no. 5766, pp. 1401–1405, Mar. 2006.
- [5] K. Konstantinidis *et al.*, "A lander mission to probe subglacial water on Saturn's moon Enceladus for life," *Acta Astronaut.*, vol. 106, pp. 63–89, Jan. 2015.
- [6] D. P. Winebrenner, W. T. Elam, V. Miller, and M. Carpenter, "A Thermal Ice-Melt Probe for Exploration of Earth-Analogs to Mars, Europa and Enceladus," presented at the Lunar and Planetary Science Conference, 2013, vol. 44, p. 2986.
- [7] M. Ono, K. Mitchell, A. Parness, K. Carpenter, and A. Curtis, "Journey to the Center of Icy Moons Phase I: Enceladus Vent Explorer Concept," JPL / Caltech, NASA Innovative Advanced Concepts (NIAC), 2017.
- [8] W. B. Sparks *et al.*, "Active Cryovolcanism on Europa?," *Astrophys. J. Lett.*, vol. 839, no. 2, p. L18, 2017.
- [9] National Research Council Committee on the Planetary Science Decadal Survey, *Vision and Voyages for Planetary Science in the Decade 2013-2022*. National Academies Press, 2012.
- [10] P. Voosen, "2.7-million-year-old ice opens window on past," *Science*, vol. 357, no. 6352, pp. 630–631, Aug. 2017.
- [11] EPICA Community Members *et al.*, "Eight glacial cycles from an Antarctic ice core," *Nature*, vol. 429, no. 10.1038/nature02599, pp. 623–628, 2004.
- [12] V. V. Petrenko, J. P. Severinghaus, E. J. Brook, N. Reeh, and H. Schaefer, "Gas records from the West Greenland ice margin covering the Last Glacial Termination: a horizontal ice core," *Quat. Sci. Rev.*, vol. 25, no. 9, pp. 865–875, May 2006.
- [13] U. Federer, P. R. Kaufmann, M. A. Hutterli, S. Schüpbach, and T. F. Stocker, "Continuous Flow Analysis of Total Organic Carbon in Polar Ice Cores,"

- Environ. Sci. Technol.*, vol. 42, no. 21, pp. 8039–8043, Nov. 2008.
- [14] M. Legrand *et al.*, “Water-soluble organic carbon in snow and ice deposited at Alpine, Greenland, and Antarctic sites: a critical review of available data and their atmospheric relevance,” *Clim. Past Katlenburg-Lindau*, vol. 9, no. 5, p. 2195, 2013.
- [15] A. Curtis and P. Kyle, “Methods for mapping and monitoring global glaciovolcanism,” *J. Volcanol. Geotherm. Res.*, 2017.
- [16] B. M. Tebo, R. E. Davis, R. P. Anitori, L. B. Connell, P. Schiffman, and H. Staudigel, “Microbial communities in dark oligotrophic volcanic ice cave ecosystems of Mt. Erebus, Antarctica,” *Front. Microbiol.*, vol. 6, Mar. 2015.
- [17] R. M. Soo, S. A. Wood, J. J. Grzymiski, I. R. McDonald, and C. S. Cary, “Microbial biodiversity of thermophilic communities in hot mineral soils of Tramway Ridge, Mount Erebus, Antarctica,” *Environ. Microbiol.*, vol. 11, no. 3, p. 715, 2009.
- [18] P. J. Boston, “Extraterrestrial Caves,” in *Encyclopedia of Cave and Karst Science*, A. Eavis, Ed. Taylor & Francis, 2004, pp. 735–741.
- [19] P. J. Boston *et al.*, “Cave biosignature suites: microbes, minerals, and Mars,” *Astrobiology*, vol. 1, no. 1, pp. 25–55, 2001.
- [20] W. M. Grundy *et al.*, “Surface compositions across Pluto and Charon,” *Science*, vol. 351, no. 6279, p. aad9189, Mar. 2016.
- [21] K. E. Fishbaugh and J. W. Head, “Comparison of the North and South Polar Caps of Mars: New Observations from MOLA Data and Discussion of Some Outstanding Questions,” *Icarus*, vol. 154, no. 1, pp. 145–161, Nov. 2001.
- [22] J. J. Petrovic, “Review Mechanical properties of ice and snow,” *J. Mater. Sci.*, vol. 38, no. 1, pp. 1–6, Jan. 2003.
- [23] R. H. Brown *et al.*, “Composition and Physical Properties of Enceladus’ Surface,” *Science*, vol. 311, no. 5766, pp. 1425–1428, Mar. 2006.
- [24] F. Scipioni *et al.*, “Deciphering sub-micron ice particles on Enceladus surface,” *Icarus*, vol. 290, no. Supplement C, pp. 183–200, Jul. 2017.
- [25] C. C. Porco *et al.*, “Cassini Observes the Active South Pole of Enceladus,” *Science*, vol. 311, no. 5766, pp. 1393–1401, Mar. 2006.
- [26] L. Poirier, E. P. Lozowski, and R. I. Thompson, “Ice hardness in winter sports,” *Cold Reg. Sci. Technol.*, vol. 67, no. 3, pp. 129–134, Jul. 2011.
- [27] J. B. Jamieson, *In situ tensile strength of snow in relation to slab avalanches*. University of Calgary, 1988.
- [28] C. Harmston, *Myths, Cautions & Techniques of Ice Screw Placement*. 1997.
- [29] A.-M. Kietzig, S. G. Hatzikiriakos, and P. Englezos, “Physics of ice friction,” *J. Appl. Phys.*, vol. 107, no. 8, p. 081101, Apr. 2010.
- [30] A. Parness, “Anchoring foot mechanisms for sampling and mobility in microgravity,” in *Robotics and Automation (ICRA), 2011 IEEE International Conference on*, 2011, pp. 6596–6599.
- [31] M. Badescu *et al.*, “Adapting the ultrasonic/sonic driller/corer for walking/climbing robotic applications,” presented at the Smart Structures and Materials 2005: Industrial and Commercial Applications of Smart Structures Technologies, 2005, vol. 5762, pp. 160–168.
- [32] H. Jiang *et al.*, “A robotic device using gecko-inspired adhesives can grasp and manipulate large objects in microgravity,” *Sci. Robot.*, vol. 2, no. 7, p. eaan4545, Jun. 2017.
- [33] J. Biele and S. Ulamec, “Capabilities of Philae, the Rosetta Lander,” *Space Sci. Rev.*, vol. 138, no. 1–4, pp. 275–289, Jul. 2008.
- [34] H. Nayar *et al.*, “Long reach sampling for ocean worlds,” in *2017 IEEE Aerospace Conference*, 2017, pp. 1–7.
- [35] J. Clark *et al.*, “Design of a Bio-inspired Dynamical Vertical Climbing Robot,” in *Robotics: Science and Systems*, 2007, vol. 1.
- [36] W. R. Provancher, S. I. Jensen-Segal, and M. A. Fehlbeg, “ROCR: An Energy-Efficient Dynamic Wall-Climbing Robot,” *IEEEASME Trans. Mechatron.*, vol. 16, no. 5, pp. 897–906, Oct. 2011.
- [37] T. Bretl, S. Rock, J.-C. Latombe, B. Kennedy, and H. Aghazarian, “Free-Climbing with a Multi-Use Robot,” in *Experimental Robotics IX*, Springer, Berlin, Heidelberg, 2006, pp. 449–458.
- [38] A. Parness *et al.*, “Gravity-independent Rock-climbing Robot and a Sample Acquisition Tool with Microspine Grippers,” *J. Field Robot.*, vol. 30, no. 6, pp. 897–915, Nov. 2013.
- [39] A. Parness, N. Abcouwer, C. Fuller, N. Wiltsie, J. Nash, and B. Kennedy, “LEMUR 3: A limbed climbing robot for extreme terrain mobility in space,” in *2017 IEEE International Conference on Robotics and Automation (ICRA)*, 2017, pp. 5467–5473.

- [40] S. Kim, A. T. Asbeck, M. R. Cutkosky, and W. R. Provancher, "SpinybotII: climbing hard walls with compliant microspines," in *ICAR '05. Proceedings., 12th International Conference on Advanced Robotics, 2005.*, 2005, pp. 601–606.
- [41] M. J. Spenko *et al.*, "Biologically inspired climbing with a hexapedal robot," *J. Field Robot.*, vol. 25, no. 4–5, pp. 223–242, Apr. 2008.
- [42] B. H. Wilcox *et al.*, "Athlete: A cargo handling and manipulation robot for the moon," *J. Field Robot.*, vol. 24, no. 5, pp. 421–434, May 2007.
- [43] M. Henrey, A. Ahmed, P. Boscariol, L. Shannon, and C. Menon, "Abigail-III: A Versatile, Bioinspired Hexapod for Scaling Smooth Vertical Surfaces," *J. Bionic Eng.*, vol. 11, no. 1, pp. 1–17, Jan. 2014.
- [44] A. Shapiro, A. Greenfield, and H. Choset, "Frictional Compliance Model Development and Experiments for Snake Robot Climbing," in *Proceedings 2007 IEEE International Conference on Robotics and Automation, 2007*, pp. 574–579.
- [45] C. Wright *et al.*, "Design and architecture of the unified modular snake robot," in *Robotics and Automation (ICRA), 2012 IEEE International Conference on*, 2012, pp. 4347–4354.
- [46] M. Minor, H. Dulimarta, G. Danghi, R. Mukherjee, R. L. Tummala, and D. Aslam, "Design, implementation, and evaluation of an under-actuated miniature biped climbing robot," in *Proceedings. 2000 IEEE/RSJ International Conference on Intelligent Robots and Systems (IROS 2000) (Cat. No.00CH37113)*, 2000, vol. 3, pp. 1999–2005 vol.3.
- [47] B. E. Shores and M. A. Minor, "Design, Kinematic Analysis, and Quasi-Steady Control of a Morphic Rolling Disk Biped Climbing Robot," in *Proceedings of the 2005 IEEE International Conference on Robotics and Automation, 2005*, pp. 2721–2726.
- [48] Y. Guan *et al.*, "Climbot: A modular bio-inspired biped climbing robot," in *2011 IEEE/RSJ International Conference on Intelligent Robots and Systems, 2011*, pp. 1473–1478.
- [49] S. Karumanchi *et al.*, "Team RoboSimian: Semi-autonomous Mobile Manipulation at the 2015 DARPA Robotics Challenge Finals," *J. Field Robot.*, vol. 34, no. 2, pp. 305–332, Mar. 2017.
- [50] German Aerospace Center, "Blood Falls – EnEx probe collects first 'clean' water samples," *DLR Portal*, 09-Feb-2015. [Online]. Available: http://www.dlr.de/dlr/en/desktopdefault.aspx/tabid-10081/151_read-12733/. [Accessed: 27-Feb-2016].
- [51] A. Fiorello, "Power ice screw system and methods of use," US9303456 B1, 05-Apr-2016.
- [52] APHA, *Standard Methods for the Examination of Water and Wastewater*. American Public Health Association., 1998.

BIOGRAPHIES



Aaron Curtis received a B.A. in geography from Cambridge University, a M.S. in geochemistry and a Ph.D. in earth science from New Mexico Institute of Mining and Technology in 2016. He has participated in seven Antarctic field seasons as lead caver for the Mount Erebus Volcano Observatory. He worked on quadcopters for physical sample collection and sensor placement at Los Alamos National Labs, served as the unmanned aerial vehicles specialist on the Trail by Fire expedition. He is currently a NASA Postdoctoral Program fellow in the Jet Propulsion Laboratory's Extreme Environment Robotics Group.



Matt Martone is an undergraduate student at Carnegie Mellon University double majoring in Mechanical Engineering and Robotics. He has interned in the rapid prototyping lab of JPL's Extreme Environment Robotics Group for two successive summers, the latter of which included his work on the ISEE mechanical design and development. He also has done research on modular snake robots and legged locomotion in the Biorobotics Lab of the Robotics Institute for the last three years. He plans to begin a PhD program in robotics after graduation.



Aaron Parness is the Group Leader of the Extreme Environment Robotics Group at JPL and the head of the Robotic Prototyping Laboratory. He received Bachelor's degrees from MIT in Mechanical Engineering and Creative Writing and an MS and PhD from Stanford University in Mechanical Engineering. Dr. Parness formulates and leads several technology development projects including work on climbing robots and robotic grippers. He and his work have been featured in the Economist, Time Magazine, and as a Popular Science Top 100 innovation of the year, as well as on the Discovery Channel, BBC, and in JPL's own Crazy Engineering YouTube series. In 2015, Dr. Parness was awarded JPL's Lew Allen Award for individual accomplishments or leadership in scientific research or technological innovation by JPL employees during the early years of their professional careers.